V. HEP BENCHMARKING ACTIVITY

(W. M. Stacey, *Georgia Tech)*

Abstract

A group of people are collaborating in the comparison experimental thermal diffusivities inferred from experimental data measured in the edge pedestal of DIII-D H-mode discharges using different codes. I am providing calculations based on a 1D edge transport code (as described in section II and Ref. 1), Rich Groebner (*General Atomics)* is providing calculations based on the 1.5D transport/MHD code ONE-TWO[2], Tarig Rafiq (*Lehigh*) is providing calculations based on the Multimode transport model in the 1.5D transport/MHD code ASTRA[3], Tom Rognlien (*Lawrence Livermore National Laboratory*) is providing calculations based on the 2D transport code UEDGE[4], and Larry Owen and John Canick (*Oak Ridge National Laboratory*) are providing calculations based on the 2D transport code SOLPS[5]. Jim Callen (*Wisconsin*) is coordinating the activity.

A. 1D Transport Calculations

My calculations for the two shots initially being considered by the group are shown in Figs 1 and 2. The edge pedestal plasma density in shot 98889 is about 1/2 of the edge density in shot 118897, as a consequence of which the neutral penetration is much greater for 98889, resulting in charge exchange being the dominant heating/cooling mechanism in the very edge for 98889 and resulting in very different heat flux profiles for the two shots. The inferred experimental chi profiles in the edge are also quite different for the two cases. The calculation procedure is described fairly succinctly in Ref. 1.

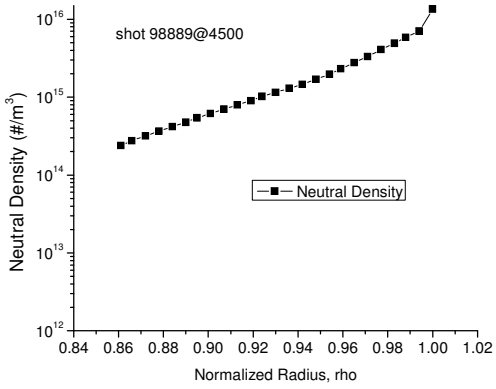

Fig. 1a Neutral Density
Shot 98889@3960

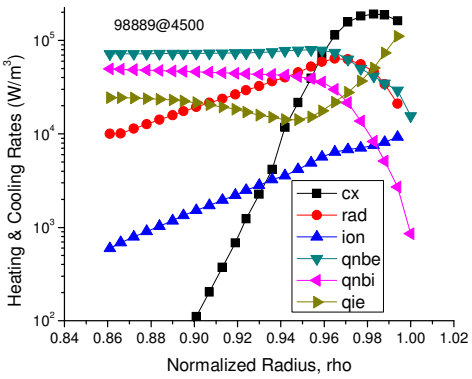

Fig. 1b Heating & Cooling Rates
Shot 98889@3960

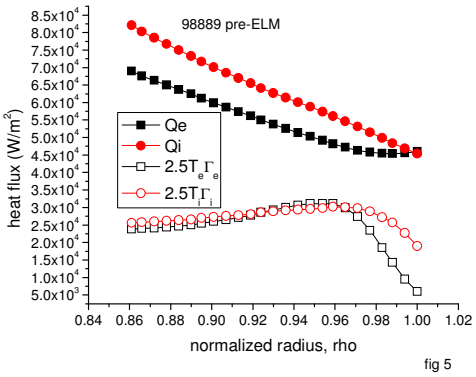

Fig. 1c Total & Convective Heat Fluxes Shot 98889@3960

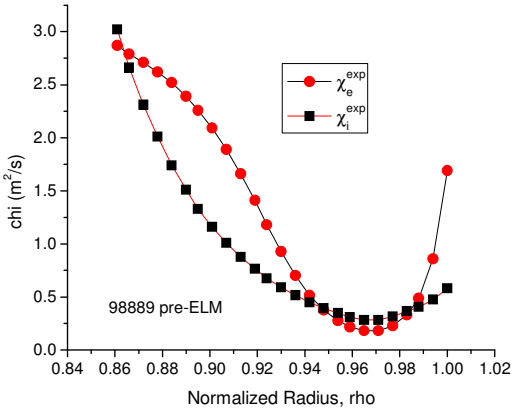

Fig. 1d χ_e & χ_i Experimental Shot 98889@3960

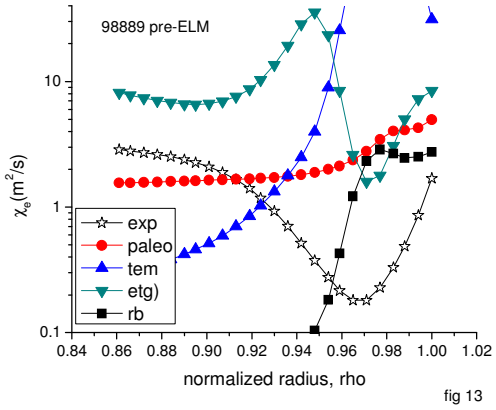

Fig. 1e Electron χ Shot 98889@3960

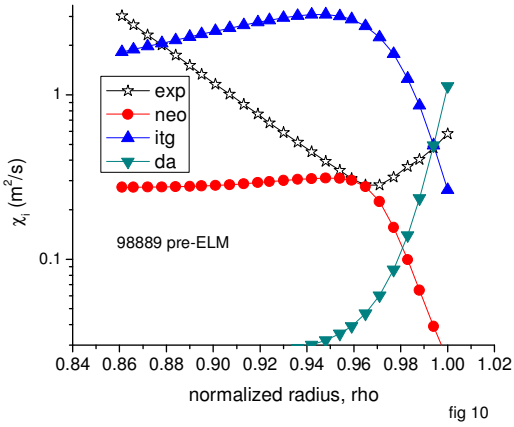

Fig.1f Ion χ Shot 98889@3960

.

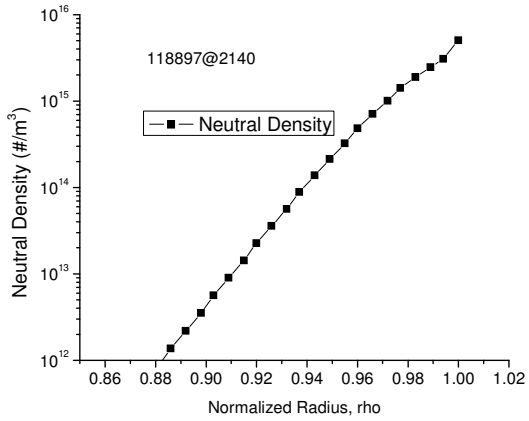

Fig. 2a Neutral Density Shot 118897@2140.

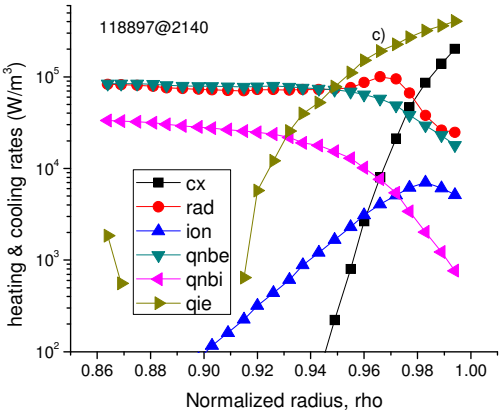

Fig. 2b Heating & Cooling Rates Shot 118897@2140.

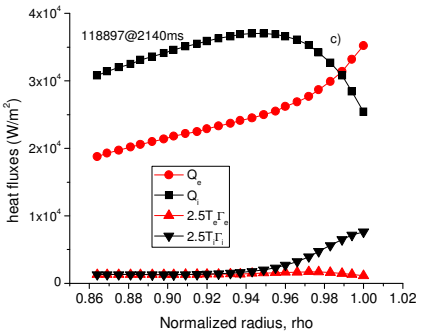

Fig. 2c Total & Convective Heat Fluxes Shot 118897@2140.

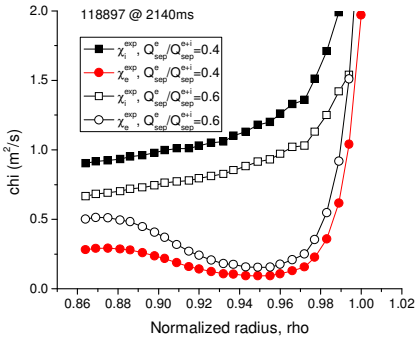

Fig. 2d. χ_e & χ_i Experimental Shot 118897@2140.

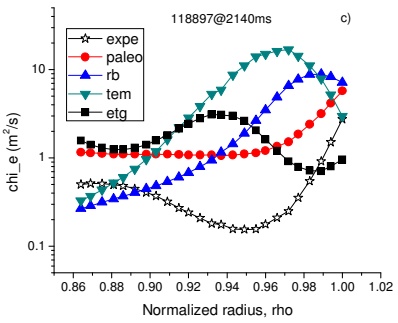

Fig. 2e Electron χ Shot 118897@2140.

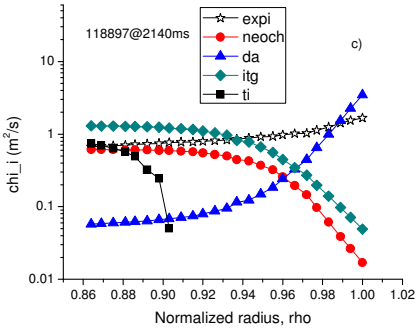

Fig. 2f Ion χ Shot 118897@2140.

B. Applications of the Miller Equilibrium to the Poloidal Variation of Temperature Gradients and Conductive Heat Fluxes

Stimulated by the relatively good agreement between the approximate formulas for the poloidal variation of the conductive heat flux that Callen derived[6] from the Miller equilibrium[7] with the calculations by the 2D codes, this formalism has been developed further, essentially retaining the dependence on triangularity and retaining an arbitrary poloidal location for measured temperature gradient in the Miller equilibrium. The result is an expression for the quantity $G(r,\theta) \equiv q(r,\theta)/\langle q(r)\rangle \equiv \langle L_T(r)\rangle / L_T(r,\theta)$ which relates the local and flux surface averaged conductive heat fluxes or temperature gradient scale lengths.

Miller equilibrium

Miller, et al.[7] derived analytical expressions for an equilibrium flux surface in a plasma as shown in Figure 3 with elongation κ, triangularity δ, and displaced centers $R_0(r)$, where r is

the half-diameter of the plasma along the midplane with center located at distance $R_0(r)$ from the toroidal centerline.

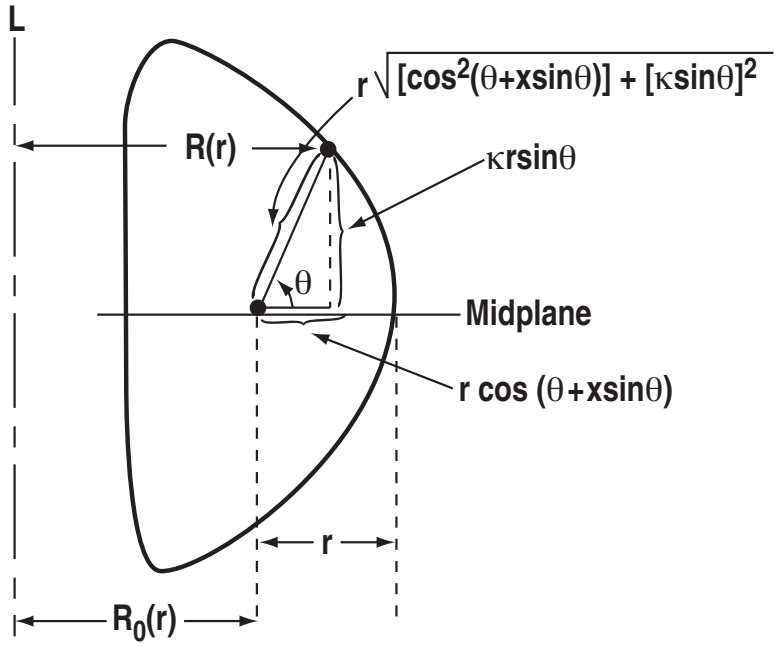

Figure 3 Miller equilibrium parameters

The R and Z coordinates of this plasma are described by[7]

$$\begin{aligned} R(r) &= R_0(r) + r\cos\left[\theta + x\sin\theta\right] \\ Z(r) &= \kappa r\sin\theta \end{aligned} \tag{1}$$

where $x \equiv \sin^{-1}\delta$.

The poloidal magnetic field in such flux surface geometry is[7]

$$\begin{aligned} RB_p &= \left|\nabla\phi\times\nabla\psi\right| = \frac{\partial\psi}{\partial r}\left|\nabla r\right| \\ &= \frac{\dfrac{\partial\psi}{\partial r}\kappa^{-1}\left[\sin^2(\theta+x\sin\theta)(1+x\cos\theta)^2 + \kappa^2\cos^2\theta\right]^{1/2}}{\cos(x\sin\theta) + \dfrac{\partial R_0}{\partial r}\cos\theta + \left[s_\kappa - s_\delta\cos\theta + (1+s_\kappa)x\cos\theta\right]\sin\theta\sin(\theta+x\sin\theta)} \end{aligned} \tag{2}$$

where $s_\kappa = \dfrac{r}{\kappa}\dfrac{\partial\kappa}{\partial r}$ and $s_\delta = r\dfrac{\partial\delta}{\partial r}/\sqrt{(1-\delta^2)}$ account for the change in elongation and triangularity, respectively, with radial location.

The shifted circle model (which leads to the Shafranov shift) yields

$$\frac{\partial R_0}{\partial r} \equiv \Delta' = -\frac{r}{R_0}\left(\beta_p + \frac{1}{2}l_i\right) \tag{3a}$$

and a shifted ellipse model by Lao, et al.[8] yields

$$\frac{\partial R_0}{\partial r} = -\frac{r}{R_0}\left[\frac{2\left(\kappa^2+1\right)}{\left(3\kappa^2+1\right)}\left(\beta_p + \frac{1}{2}l_i\right) + \frac{1}{2}\frac{\left(\kappa^2-1\right)}{\left(3\kappa^2+1\right)}\right] \tag{3b}$$

Flux surface average

The flux surface average (FSA) of a quantity $A(r,\theta)$ in this flux surface geometry is

$$\left\langle A(r,\theta)\right\rangle \equiv \frac{\oint \frac{A(r,\theta)dl_p}{B_p}}{\oint \frac{dl_p}{B_p}} = \frac{\oint A(r,\theta)\,z(r,\theta)\,dl_p}{\oint z(r,\theta)\,dl_p} \tag{4}$$

where

$$z(r,\theta) \equiv \frac{\cos\left(x\sin\theta\right) + \frac{\partial R_0}{\partial r}\cos\theta + \left[s_\kappa - s_\delta\cos\theta + (1+s_\kappa)x\cos\theta\right]\sin\theta\sin\left(\theta + x\sin\theta\right)}{\left[\sin^2\left(\theta+x\sin\theta\right)\left(1+x\cos\theta\right)^2 + \kappa^2\cos^2\theta\right]^{1/2} \Big/ \left[R_0(r) + r\cos\left[\theta + x\sin\theta\right]\right]} \tag{5}$$

and the differential poloidal length is (see Fig. 3)

$$dl_p = r\sqrt{\left[\cos^2\left(\theta + x\sin\theta\right) + \kappa^2\sin^2\theta\right]}\,d\theta \tag{6}$$

Equivalent toroidal models

Simple toroidal models are widely used for transport calculations and experimental data interpretation (e.g Ref. 1). The usual flux surface model implicitly assumed in such codes, which will be referred to as the "elliptical" model" is (e.g. Ref. 1) $R = R_0 + r\cos\theta, Z = \kappa r\sin\theta$, $B_p = B_{p0}\Big/\left(1+\frac{r}{R_0}\cos\theta\right)$. The usual approach is to construct an effective toroidal or cylindrical model that preserves the area of flux surface, which for this model leads to a relation between the effective radius variable $\bar{r}$ of the equivalent torus and the actual radial variable in the horizontal midplane r given in the elliptical model by $\bar{r} = r\sqrt{\frac{1}{2}\left(1+\kappa^2\right)}$.

Such equivalent models should be improved by using instead the Miller equilibrium. The area of the flux surface ψ passing through the midplane radius r is

$$A(\psi) = \oint_{\psi} dl_p \int_0^{2\pi} h_\phi d\phi = 2\pi \oint_{\psi} R dl_p$$
$$= 2\pi r R_0(r) \int_0^{2\pi} \left[1 + \frac{r}{R_0(r)} \cos(\theta + x \sin\theta)\right] \left[\cos^2(\theta + x\sin\theta) + \kappa^2 \sin^2\theta\right]^{1/2} d\theta \quad (7)$$

The area of a cylinder with radial variable $\bar{r}$ is $A_c(\bar{r}) = 2\pi R_0(a) 2\pi \bar{r}$. Equating the two areas and solving for

$$\bar{r} = r \frac{R_0(r)}{2\pi R_0(a)} \int_0^{2\pi} \left[1 + \frac{r}{R_0(r)} \cos(\theta + x\sin\theta)\right] \left[\cos^2(\theta + x\sin\theta) + \kappa^2 \sin^2\theta\right]^{1/2} d\theta \quad (8)$$

defines the radial variable of an equivalent cylinder that preserves the surface area of the Miller equilibrium flux surface.

A comparison calculation was made for a plasma representative of shot 98889 with minor horizontal radius a = 0.583 m, varying triangularity, elongation $\kappa = 1.75$, and major radius $R_0(a) = 1.77m$. The elliptical model predicts for these parameters an effective circular plasma radius $\bar{a} = 0.830\,m$. Evaluation of Eq. (8) with $x = \sin^{-1}\delta$ yields almost the same value of $\bar{a} = 0.817m$ for $\delta = 0$, as shown in Table 1. For non-zero values of the triangularity, the Miller model predicts increasingly smaller equivalent cylindrical radii than the elliptical model to preserve surface area.

Table 1 Effect of triangularity on effective cylindrical radius and $G(a, \theta = 0)$

δ triangularity	$\bar{a}(m)$ Miller equil.	$\bar{a}(m)$ elliptic equil	$G(a,\theta=0)$ Miller equil.	$G(a,\theta=0)$ elliptic equil
0.0	0.817	0.830	1.73	1.43
0.1	0.800	"	1.73	"
0.2	0.784	"	1.73	"
0.3	0.769	"	1.73	"
0.4	0.753	"	1.72	"
0.5	0.739	"	1.71	"
0.6	0.725	"	1.69	"
0.7	0.710	"	1.66	"
0.8	0.696	"	1.62	"
0.9	0.680	"	1.55	"

Interpretation of thermal conductivities from measured temperature gradients

Another application of the Miller equilibrium that immediately comes to mind is in the inference of experimental thermal diffusivities from measured temperature gradients in tokamaks. The measured temperature gradient $(dT/dr)_{\exp}$ pertains of course to the location $\left(r,\theta_{\exp}\right)$ at which the measurement is made (although sometimes it is mapped along flux surfaces to another location such as the outboard midplane at $\left(r,\theta=0\right)$). On the other hand, one-dimensional radial transport codes calculate an average conductive heat flux $<q\left(r\right)>$. In order to use the calculated average heat flux and the local (in θ) measured temperature gradient in the heat conduction relation to infer a measured thermal diffusivity $\chi=-q/n\left(dT/dr\right)\equiv qL_T/nT$, the local temperature gradient scale length must be mapped into an average value over the flux surface

$$\begin{aligned}(L_T)_{\exp}&\equiv -T(dr/dT)_{\exp}\Rightarrow <L_T>=-T\left(dr/dT\right)_{\exp}\left(<dr>/dr\left(\theta_{\exp}\right)\right)\\&\equiv\left(L_T\right)_{\exp}\left(<dr>/dr\left(\theta_{\exp}\right)\right)=\left(L_T\right)_{\exp}\left(\left|\nabla r\left(\theta_{\exp}\right)\right|/<\left|\nabla r\right|>\right)\end{aligned} \tag{9}$$

From Eq. (2), the local $\left|\nabla r\right|$ may be written

$$\left|\nabla r\left(r,\theta\right)\right|=\frac{\kappa^{-1}\left[\sin^2\left(\theta+x\sin\theta\right)\left(1+x\cos\theta\right)^2+\kappa^2\cos^2\theta\right]^{1/2}}{\cos\left(x\sin\theta\right)+\dfrac{\partial R_0}{\partial r}\cos\theta+\left[s_\kappa-s_\delta\cos\theta+(1+s_\kappa)x\cos\theta\right]\sin\theta\sin\left(\theta+x\sin\theta\right)} \tag{10}$$

Using this in Eq. (4) yields an expression for the FSA value

$$\left\langle\left|\nabla r\left(r\right)\right|\right\rangle=\frac{\int_0^{2\pi}\left[R_0\left(r\right)+r\cos\left(\theta+x\sin\theta\right)\right]\left[\cos^2\left(\theta+x\sin\theta\right)+\kappa^2\sin^2\theta\right]^{1/2}d\theta}{\int_0^{2\pi}F\left(r,\theta\right)\left[R_0\left(r\right)+r\cos\left(\theta+x\sin\theta\right)\right]\left[\cos^2\left(\theta+x\sin\theta\right)+\kappa^2\sin^2\theta\right]^{1/2}d\theta} \tag{11}$$

where

$$F\left(r,\theta\right)=\frac{\cos\left(x\sin\theta\right)+\dfrac{\partial R_0}{\partial r}\cos\theta+\left[s_\kappa-s_\delta\cos\theta+(1+s_\kappa)x\cos\theta\right]\sin\theta\sin\left(\theta+x\sin\theta\right)}{\kappa^{-1}\left[\sin^2\left(\theta+x\sin\theta\right)\left(1+x\cos\theta\right)^2+\kappa^2\cos^2\theta\right]^{1/2}} \tag{12}$$

The FSA value of the temperature gradient scale length, $\left\langle L_T\right\rangle=-\left\langle T/\left(dT/dr\right)\right\rangle$, which is the quantity needed for the inference of experimental thermal diffusivity using the average heat

flux calculated by 1D transport codes, is related to the local value of the temperature gradient scale length, $L_T(\theta) = -T(\theta)/(dT/dr)_\theta$, which is the quantity measured, by

$$\frac{\langle L_T(r)\rangle}{L_T(r,\theta)} = \frac{|\nabla r(r,\theta)|}{\langle|\nabla r(r)|\rangle} \equiv G(r,\theta) \tag{13}$$

For the case $\theta = 0$, corresponding to the outboard midplane location of the measured gradient scale lengths, Eq. (10) reduces to the Shafranov shift correction

$$|\nabla(r,\theta=0)| = \frac{1}{\left(1+\partial R_0/\partial r\right)} \tag{14}$$

A series of calculations was performed for the same plasma model (representative of shot 98889) with minor horizontal radius a = 0.583 m, varying triangularity, elongation $\kappa = 1.75$, and major radius $R_0(a) = 1.77m$, using Eqs. (10)-(13) with $s_\kappa = 0, s_\delta = 0$ and using the elliptical model discussed in the previous section, for which $G(r,\theta=0) = \sqrt{\frac{1}{2}\left(1+\kappa^2\right)}$. The results are shown in Table 1. The Miller model predicts values of $G(a,\theta=0)$ that are 10-20% larger than those predicted by the elliptical model.

Neglecting the effect of the radial variation of the elongation and triangularity ($s_\kappa = 0, s_\delta = 0$) and also momentarily neglecting the triangularity ($\delta = 0$), reduces Eq. (13) to a form that more readily exhibits the various factors involved

$$\frac{\langle L_T(r)\rangle}{L_T(r,\theta=0)} = G(r,\theta=0) = \frac{\int_0^{2\pi} \frac{\kappa\left[1+\frac{\partial R_0}{\partial r}\cos\theta\right]}{\left[1+\left(\kappa^2-1\right)co\,s^2\,\theta\right]^{1/2}}\left[R_0+r\cos\theta\right]\left[1+\left(\kappa^2-1\right)\sin^2\theta\right]^{1/2} d\theta}{\left[1+\frac{\partial R_0}{\partial r}\right]\int_0^{2\pi}\left[R_0+r\cos\theta\right]\left[1+\left(\kappa^2-1\right)\sin^2\theta\right]^{1/2} d\theta} \tag{15}$$

Prediction of poloidal distribution of conductive heat flux

One-dimensional transport codes calculate an average conductive heat flux, $\langle q\rangle$, over the flux surface. Assuming that the density, temperature and thermal diffusivity are uniform over the flux surface, the poloidal dependence of the conductive heat flux must arise through the poloidal dependence of the radial temperature gradient

$$q(r,\theta) = n(r)T(r)\chi(r)L_T^{-1}(r,\theta) = n(r)T(r)\chi(r)\left\langle L_T(r)\right\rangle^{-1} G(r,\theta) \qquad (16)$$

The value of $G(r,\theta) \equiv q(r,\theta)/\left\langle q(r)\right\rangle \equiv \left\langle L_T(r)\right\rangle / L_T(r,\theta)$ calculated from Eqs. (10)-(13) at the separatrix $(r \to a)$ of the model problem previously described $(\Delta' = -0.25, \kappa = 1.75, r/R = 1/3)$ is plotted in Fig. 4 The curve labeled symmetric uses averaged values $\kappa = 1.77, \delta = 0.14$ for all values of θ, while the curve labeled asymmetric uses experimental values $\kappa_{top} = 1.50, \delta_{top} = 0.0$ in the upper half $0 \le \theta \le \pi$ and $\kappa = 2.32, \delta = 0.14$ in the lower half $\pi \le \theta \le 2\pi$.

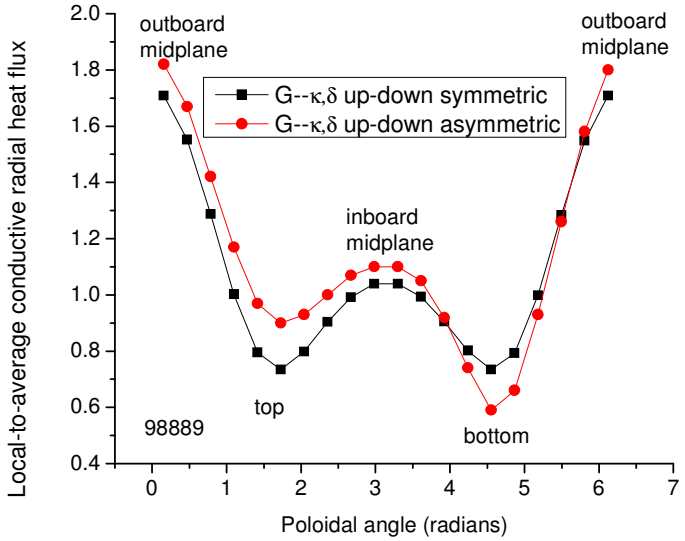

Figure 4 Predicted poloidal distribution of the conductive heat flux at the separatrix for a DIII-D shot 98889 model.

Relation to various HEP benchmarking calculations

The 2D codes (UEDGE[4] and SOLPS[5]) calculate $q(r,\theta_{\exp})$ at the location of the measured temperature gradient $L_T(r,\theta_{\exp})$ directly, and the two quantities can be directly combined to infer the experimental thermal diffusivity $\chi_{\exp} \equiv q(r,\theta_{\exp})L_T(r,\theta_{\exp})/nT$.

The 1.5D (2D MHD, 1D transport) codes (ONE-TWO[2] and ASTRA[3]) use the calculated 2D MHD equilibrium to construct an equivalent 1D transport model, from which is calculated a FSA value of $\left\langle q(r)\right\rangle$. In order to evaluate the experimental thermal diffusivity, it is then necessary either to map this average heat flux to a local value at the location of the measurement, $q(r,\theta_{\exp}) = G(r,\theta_{\exp})\left\langle q(r)\right\rangle$ or equivalently to map the measured value of the temperature gradient to an average value over the flux surface, $\left\langle L_T(r)\right\rangle = G(r,\theta_{\exp})L_T(r,\theta_{\exp})$. In either

case, the resulting expression for the inferred experimental thermal diffusivity is $\chi_{\exp} \equiv G\left(r,\theta_{\exp}\right)\left\langle q\left(r\right)\right\rangle L_T\left(r,\theta_{\exp}\right)/nT$. The 2D MHD calculation in principle uses the quantities necessary to evaluate the mapping function $G\left(r,\theta_{\exp}\right)$. Alternatively, this function can be evaluated from the Miller equilibrium or the simpler elliptical equilibrium.

The 1D codes[1] use an effective cylinder with radius $\bar{r} = r\sqrt{\left(1+\kappa^2\right)/2} = 1.4r$ (which preserves the surface area of an elliptical equilibrium with elongation κ) to calculate a FSA value of $\left\langle q\left(r\right)\right\rangle$. In this approximation $\left\langle L_T\left(r\right)\right\rangle / L_T\left(r,\theta_{\exp}=0\right) = \bar{a}/a = \sqrt{\left(1+\kappa^2\right)/2} = 1.4$. Using the improved Miller approximation that retains triangularity dependence, rather than the elliptical approximation, results in an equivalent radius about 7% smaller, hence a heat flux about 7% larger, than with the elliptical approximation. The Miller equilibrium also leads to $\left\langle L_T\left(r\right)\right\rangle / L_T\left(r,\theta_{\exp}=0\right) = 1.7$, instead of the elliptical value of 1.4. Thus, using the Miller equilibrium instead of the elliptical equilibrium in the 1D calculations[1] would be roughly estimated to increase the inferred thermal diffusivities $\chi_{\exp} = \left\langle q\right\rangle\left\langle L_T\right\rangle / nT$ by about 30% for the parameters that characterize the benchmark problems. Note that Callen's formula[6] yields a somewhat smaller value of $\left\langle L_T\left(r\right)\right\rangle / L_T\left(r,\theta_{\exp}=0\right) = \sqrt{S(r,\theta=0)} = \sqrt{\frac{2\kappa^2}{\left(1+\kappa^2\right)}\left(1-2\Delta'\right)} = 1.5.$

References

1. W. M. Stacey and R. J. Groebner, Phys. Plasmas, 13, 072510 (2006); 14, 012501 (2007).
2. H. L. St. John, "Equations and Associated Definitions used in ONE-TWO", General Atomics report (2005).
3. J. Kinsey and G. Bateman, Phys. Plasmas, 3, 3344 (1996).
4. T. D. Rognlien, D. D. Ryutov, N. Mattor and G. D. Porter, Phys. Plasmas, 5, 1851 (1999); Contrib. Plasma Phys., 38, 152 (1998); Plasma Phys. Control. Fusion, 47, A283 (2005)
5. V. A. Rozhansky, S. P. Voskoboynikov, E. G. Kaveeva, D. P. Coster and R. Schneider, Nucl. Fusion, 41, 387 (2001);42, 1110 (2002); 43, 614 (2003); Contrib. Plasma Phys., 46,575 (2006).
6. J. D. Callen,"Poloidal Variation of Radial Heat Flow in Tokamak Edge Plasmas" University of Wisconsin report (2008).
7. R. L. Miller, M.S. Chu, J. M. Greene, et al., Phys. Plasmas, 5, 973 (1998).
8. L. L. Lao, S. P. Hirshman and J. Wieland, Phys. Fluids, 24, 1431 (1981).